Infrared Physics & Technology 66 (2014) 152–159

Contents lists available at ScienceDirect

Infrared Physics & Technology

journal homepage: www.elsevier.com/locate/infrared

Variational infrared image enhancement based on adaptive dual-threshold gradient field equalization

Wenda Zhao [a,b], Zhijun Xu [a,*], Jian Zhao [a], Fan Zhao [a,b], Xizhen Han [a]

[a] Changchun Institute of Optics, Fine Mechanics and Physics, Chinese Academy of Sciences, Changchun 130033, China
[b] University of Chinese Academy of Sciences, Beijing 100049, China

HIGHLIGHTS

- Transforming the infrared image into its gradient domain to get the gradient histogram.
- The gradient field equalization with dual-threshold is obtained using the histogram equalization technique.
- Adopting the total variational model while constructing the objective function.
- Using the variational method, the enhanced image is reconstructed from the target gradient field.

ARTICLE INFO

Article history:
Received 24 February 2014
Available online 19 June 2014

Keywords:
Images processing
Infrared image enhancement
Gradient histogram equalization
Adaptive dual-threshold
Total variation

ABSTRACT

Infrared images are characterized by low signal to noise ratio (SNR) and fuzzy texture edges. This article introduces the variational infrared image enhancement algorithm based on gradient field equalization with adaptive dual thresholds. Firstly, we transform the image into gradient domain and get the gradient histogram. Then, we do the gradient histogram equalization. By setting adaptive dual thresholds to qualify the gradients, the image is prevented from over enhancement. The total variation (TV) model is adopted in the reconstruction of the enhanced image to suppress noise. It is shown from experimental results that the image edge details are significantly enhanced, and therefore the algorithm is qualified for enhancement of infrared images in different applications.

1. Introduction

Infrared images are widely applied in military, scientific, medical and other fields. However, infrared images have shortcomings of noise, low contrast and blurred texture details due to the uneven photosensitive response of infrared detector and non-ideal optics system. These affect the application of infrared images. To give qualified image information in applications, it is necessary to enhance the faint edge details of infrared images [1–3].

The technique of histogram equalization (HE) is an important method for enhancing image details [4–6]. It makes the image gray level values to appear approximately equally distributed in the corresponding histogram, which extends the dynamic range of the image. However, it is easy to produce over-enhancement, where the background noise with typical gray level values gets amplified while the detailed information with typical gray level values is constrained. To overcome the shortcomings of HE, many improvements have been proposed such as platform histogram equalization (PHE) [7] and double platform histogram equalization (DPHE) [8]. They suppress background noise by setting one or two platform thresholds. For infrared image enhancement, there are some other methods, such as using multiscale new top-hat transform [9], multi-scale decomposition [10] and human visual system [11]. In recent years, the method of variational partial differential equations (VPDE) [12–14] is applied to image enhancement by many scholars. They design the adaptive diffusion coefficients by judging whether smoothing or enhancing of different pixels to achieve image enhancement.

Local changes of image often correspond to the edge details information. In VPDE theory, the local variations of images can be expressed using the corresponding gradients. If the gradient value is large, image edge texture details will be clear. In this paper, we enhance infrared image edge details by the transformation of gradient field. The histogram equalization technology is applied to image gradient domain, increasing the small gradient values to enhance image texture details while suppressing the large gradient values to prevent over-enhancement. In order to

* Corresponding author. Tel.: +86 0431 86176577.
E-mail address: xuzj538@ciomp.ac.cn (Z. Xu).

http://dx.doi.org/10.1016/j.infrared.2014.05.018
1350-4495/

improve the SNR of infrared images, we adopt the TV constraint in constructing the objective function. Therefore, the proposed algorithm effectively enhances infrared image edge details while suppressing noise.

2. The proposed method

In this section, a novel enhancement algorithm of infrared image texture details is proposed. The process of this algorithm includes four steps. Fig. 1 shows the framework of this method.

The following subsections give a detailed description of each part of the algorithm respectively.

2.1. Gradient field equalization with adaptive dual-threshold

To a point $p(x,y) \subset \Omega$ of the infrared image $I(x,y((x,y) \subset \Omega = [0, N-1] \times [0, M-1])$, where Ω represents the size of the image, and N and M are the length and width of the image, respectively, the gradient $\nabla p(x,y)$, gradient magnitude value $|\nabla p(x,y)|$ and gradient direction θ are defined as:

$$\nabla p(x,y) = \left[\frac{\partial p(x,y)}{\partial x}, \frac{\partial p(x,y)}{\partial y}\right] \tag{1}$$

$$|\nabla p(x,y)| = \sqrt{\left|\frac{\partial p(x,y)}{\partial x}\right|^2 + \left|\frac{\partial p(x,y)}{\partial y}\right|^2} \tag{2}$$

$$\theta = \arctan\left[\left|\frac{\partial p(x,y)}{\partial y}\right| \Big/ \left|\frac{\partial p(x,y)}{\partial x}\right|\right] \tag{3}$$

where ∇ is the gradient operator, $\nabla p(x,y)$ reflects the changes of adjacent gray level values of $p(x,y)$, $|\nabla p(x,y)|$ indicates the size of the changes and θ indicates the direction of the maximum change of gray level values. So, gradients of each point of the image form a vector field, which is the gradient field. We calculate the histogram of the image using the gradient values instead of the gray level values. In the histogram, the horizontal axis represents the gradient values and ordinate represents the frequency of the gradient values (the number of pixels). Fig. 2 shows an example of gradient magnitude field and gradient histogram of the infrared image.

To infrared images, most of the gradient values are small. And in the gradient histogram, the small gradient values have a high probability. However, the histogram equalization technology just tends to enhance the high probability information, increasing the small gradient values. Therefore, gradient histogram equalization can enhance the faint edge details. Gradient histogram equalization is defined as Eq. (4),

$$\begin{cases} s_k^g = \sum_{j=0}^{k} P_r(r_j^g) = \sum_{j=0}^{k} \frac{n_j}{n} \\ k = 0, 1, \ldots, |\nabla u_0|_{\max} - 1 \end{cases} \tag{4}$$

where s_k^g means the transformed probability which corresponded to the gradient value k, n is the total number of image pixels, $|\nabla u_0|_{\max}$ means the maximum gradient value, n_j means the number of gradient value j and $P_r(r_j^g)$ means the probability of the gradient value j. Equalization image $E^g[|\nabla u_0|]$ is expressed as Eq. (5):

$$E^g[|\nabla u_0|] = \left[\sum_{j=0}^{u_0^g(x,y)} P_r(r_j)\right] \cdot |\nabla u_0|_{\max} = \left(\sum_{j=0}^{u_0^g(x,y)} \frac{n_j}{n}\right) \cdot |\nabla u_0|_{\max} \tag{5}$$

where $u_0^g(x,y)$ represents gradient values of the image u_0. Gradient field of the image u_0 after equalization is represented as:

$$\mathbf{E} = \frac{\nabla u_0}{|\nabla u_0|} \cdot E^g[|\nabla u_0|] \tag{6}$$

where $\mathbf{E}$ is the gradient field after equalization, u_0 is the original image, $|\nabla u_0|$ stands for the gradient value of u_0, $E^g[|\nabla u_0|]$ represents the gradient histogram equalization and $\frac{\nabla u_0}{|\nabla u_0|}$ is to keep the direction of image gradient field unchanged.

For gradient field equalization, the enhancement effect is obvious to the image whose gradient values are uniform distribution. But for the infrared image with low contrast and fuzzy edge details, the gradient histogram shape is a narrow single peak and the gradient values are small. As shown in Fig. 2(c), the gradient values are about 0–50. Because the gradient histogram equalization makes the image gray level values to appear approximately equally distributed in the corresponding histogram, it excessively extends the dynamic range of the gradient values. So the enhancement image, reconstructed from the equalization gradient field, produces white spots due to the over-enhancement. Fig. 3 is an example of image enhancement. Fig. 3(a) is the gradient magnitude after equalization of the original image in Fig. 2(a), and Fig. 3(b) is the correspondent gradient histogram. It can be seen that the gradient values are extended to 0–200. So the reconstructed image is sharpened and has white spots as shown in Fig. 3(c).

In order to overcome above problem of gradient field equalization, we set two adaptive thresholds to increase small gradient values while suppressing the large gradient values. In this way the revised gradient values after histogram equalization are extended to 0–110 as shown in Fig. 3(e). Thus the reconstructed image has clear edge details and the over-enhancement is avoided, as shown in Fig. 3(f). This can also be seen from the gradient magnitude (Fig. 3(a) and (d)), where the revised gradient magnitude is not excessively enhanced. The revised gradient value is expressed as follows:

$$g' = \begin{cases} g_1 & |\nabla u_0| < g_1 \\ |\nabla u_0| & g_1 \leqslant |\nabla u_0| \leqslant g_2 \\ g_2 & |\nabla u_0| > g_2 \end{cases} \tag{7}$$

where g' represents revised gradient value, and g_1 and g_2 represent adaptive thresholds. To the selection of upper threshold g_2, if g_2 is too large, it will not effectively limit the high gradient value, and cannot prevent over-enhancement; if g_2 is too small, it will restrict the enhancement of image texture details. Therefore, this article makes g_2 less than the maximum gradient of image and greater than the average value of the maximum gradient of each column. The lower threshold g_1 is to enhance small targets and weak edge detail information. If g_1 is too small, the targets and weak edge

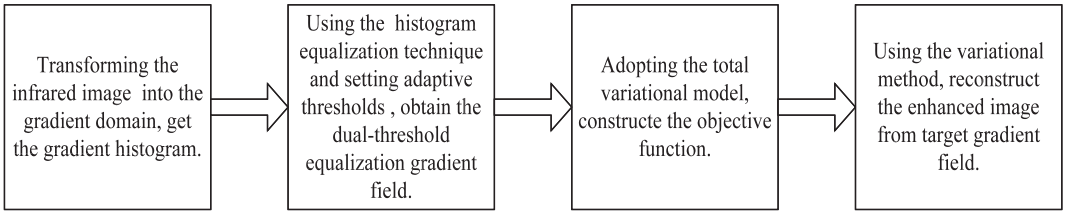

Fig. 1. The framework of infrared image texture details enhancement method.

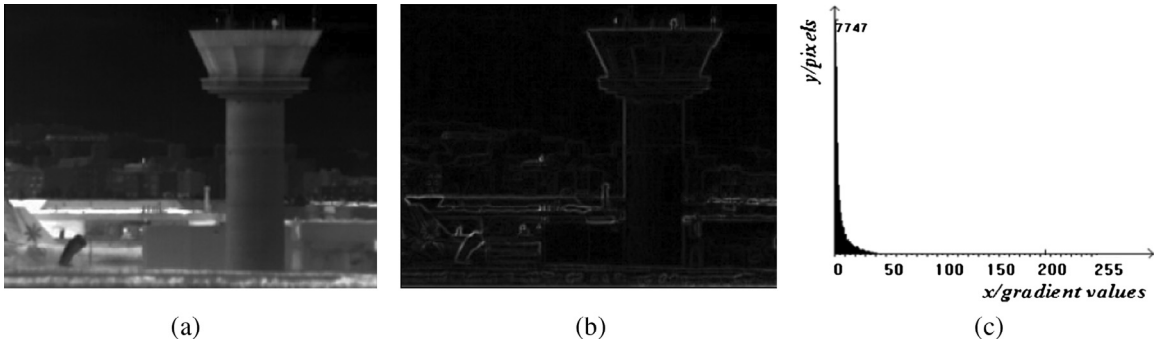

Fig. 2. Example of gradient magnitude field and gradient histogram, (a) original infrared image, (b) gradient magnitude field and (c) gradient histogram.

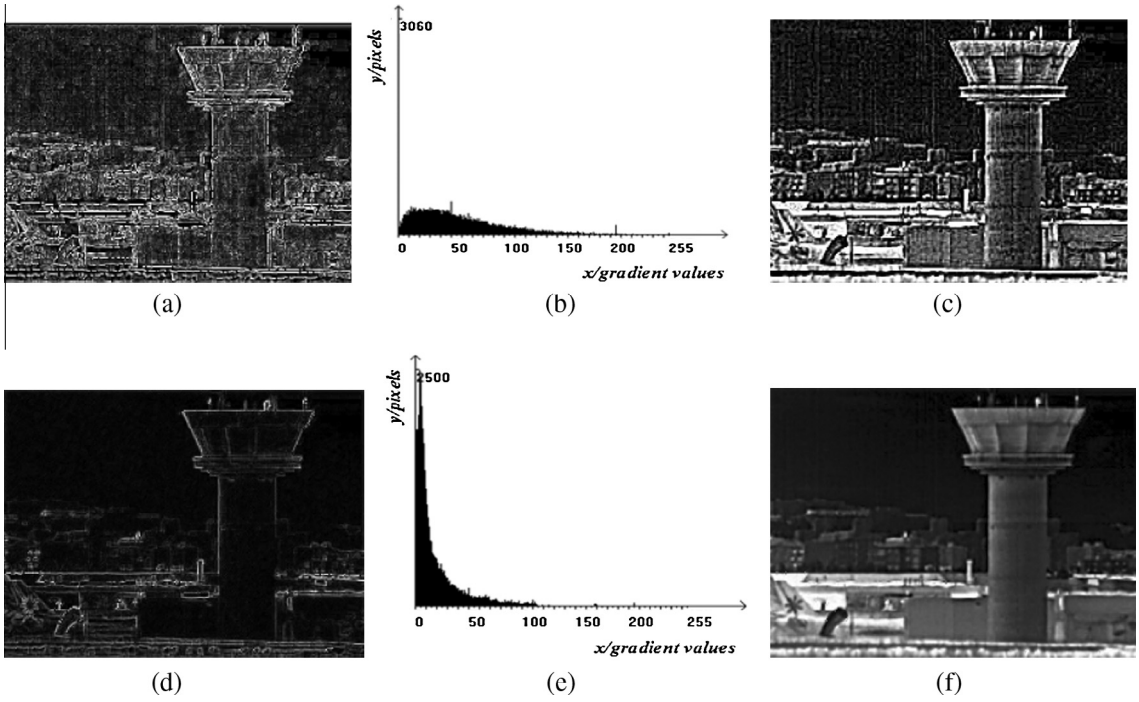

Fig. 3. The example of image enhancement, (a) gradient magnitude after equalization, (b) gradient histogram after equalization, (c) reconstructed image of (a), (d) revised gradient magnitude after equalization, (e) revised gradient histogram after equalization and (f) reconstructed image of (d).

detail information will not be significantly enhanced; if g_1 is too big, the image texture edges will be sharpened excessively. Therefore, based on the characteristics of infrared image, the calculation steps of g_1 and g_2 are as follows:

- Step 1: calculating the gradient values $\{g(i,j)|1 \leqslant i \leqslant N, 1 \leqslant j \leqslant M.\}$ of all pixels of the original image.
- Step 2: calculating the maximum gradient values $\{g_{\max}(j)|1 \leqslant j \leqslant M\}$ of each column.
- Step 3: from $\{g_{\max}(i)|1 \leqslant i \leqslant M\}$, calculating the minimum gradient value $g_{\min}$, the maximum gradient value $g_{\max}$ and the average gradient value $\bar{g}$.
- Step 4: calculating the lower threshold $g_1 = g_{\min}/2$ and the upper threshold $g_2 = (g_{\max} + 2 \cdot \bar{g})/3$.

The revised gradient histogram equalization is expressed as follows:

$$\mathbf{E}' = \frac{\nabla u_0}{|\nabla u_0|} \cdot E^g[g'] \tag{8}$$

where $\mathbf{E}'$ is gradient field of revised gradient histogram equalization, and $E^g[g']$ represents the revised gradient histogram equalization.

2.2. Rebuild the enhanced image from the gradient field $\mathbf{E}'$

Now we have obtained the transform of gradient field $\mathbf{E}'$. To find an image f, whose gradient field is equal to $\mathbf{E}'$, an intuitive idea is to solve the equation $\nabla f = \mathbf{E}'$. However, usually it has no solution because $\mathbf{E}'$ constructed from (8) may not be integrable, and there will not exist an infrared image who has the exact edge textures information as $\mathbf{E}'$. A common method for this problem is to find a closest image u, whose gradients have the least-squared-error to $\mathbf{E}'$. Using mathematical formula, the following function can be minimized:

$$\min \int\int_{\Omega} |\nabla u - \mathbf{E}'|^2 dxdy \tag{9}$$

Normally, the noise of infrared images is obvious. To enhance image details while suppressing noise, we adopt the TV model [15]. Rudin et al. think the total variation value of noisy images is bigger than that of the noiseless images, and the minimization of the total variation value of the image u can suppress noise. The TV model is represented as follows:

$$\min \int \int_{\Omega} |\nabla u| dxdy \tag{10}$$

Comprehensively considering the image edge details and noise suppression, to reconstruct the enhanced image u from the gradient field $\mathbf{E}'$, we can minimize the following functional:

$$E(u) = \min \left\{ \chi \int \int_{\Omega} |\nabla u| dxdy + \delta \int \int_{\Omega} |\nabla u - \mathbf{E}'|^2 dxdy \right\} \tag{11}$$

where u is the enhanced image, $E(u)$ is the objective function, and parameters χ and δ adjust the proportion of the two parts above. However, TV model is easy to make the enhanced image have staircase effect [16], and in order to reduce this effect, χ should be smaller than δ. With the variational method, the Euler–Lagrange equation of (11) is as:

$$\chi \nabla \cdot \left[\frac{\nabla u}{|\nabla u|} \right] + 2\delta(\Delta u - div\mathbf{E}') = 0 \tag{12}$$

where Δ is the Laplace operator, $\Delta u = \frac{\partial^2 u}{\partial x^2} + \frac{\partial^2 u}{\partial y^2}$. Minimization of the solution of (11) can be achieved by gradient descent method iterations, such as (13):

$$u^{n+1} = u^n - \Delta t \left[\chi \nabla \cdot \left[\frac{\nabla u^n}{|\nabla u^n|} \right] + 2\delta(\Delta u^n - div\mathbf{E}') \right] \tag{13}$$

where n represents the number of iterations, and Δt represents the time step, which should be a small positive number to ensure the convergence of (13).

The range of image values must sit between [0, 255] to be displayed on the computer. Therefore, each iteration should be reconstrained as follows:

$$\begin{cases} u_{temp} = u^n - \Delta t \left\{ \chi \nabla \cdot \left[\frac{\nabla u^n}{|\nabla u^n|} \right] + 2\delta(\Delta u^n - div\mathbf{E}') \right\} \\ u^{n+1} = \max\{0, \min(255, u_{temp})\} \end{cases} \tag{14}$$

The process of image reconstruction is shown in Fig. 4.

3. Experiment results and discussion

$E(u)$ of (11) may not be satisfied with convexity, so iterations of (14) may not converge. If we take the input image u_0 as the initial iteration value u^0, the optimum result u can be obtained. Fig. 5 shows the relationship between mean gradient [17] (MG) of enhanced images and the number of iterations n.

In Fig. 5, MG gradually increases as n increases from zero, until it reaches its maximum value of 16. When $n = 80$, MG decreases gradually. This phenomenon indicates that we can find the optimum result through limited iterations. In theory, image edge details are clear if MG is large. Therefore, when $n = 25$, corresponding to the maximum MG, we can find that the image edge details are the most clear. However, with M increases, the computing time of the algorithm will be longer. Comprehensively consider real-time performance of the algorithm and visual effects of the image, we take $n = 6$.

In order to intuitively show the influence of the number of iterations on the reconstructed image, we give another comparative experiment of the infrared face images [18] reconstructed by different n, as shown in Fig. 6.

Fig. 6(a) is an infrared face image with fuzzy edges. From Fig. 6(b)–(d), the contrast of the reconstructed image increases as n increases. When $n = 6$, the image edge details are clear; but when $n = 80$, the image is over-enhanced.

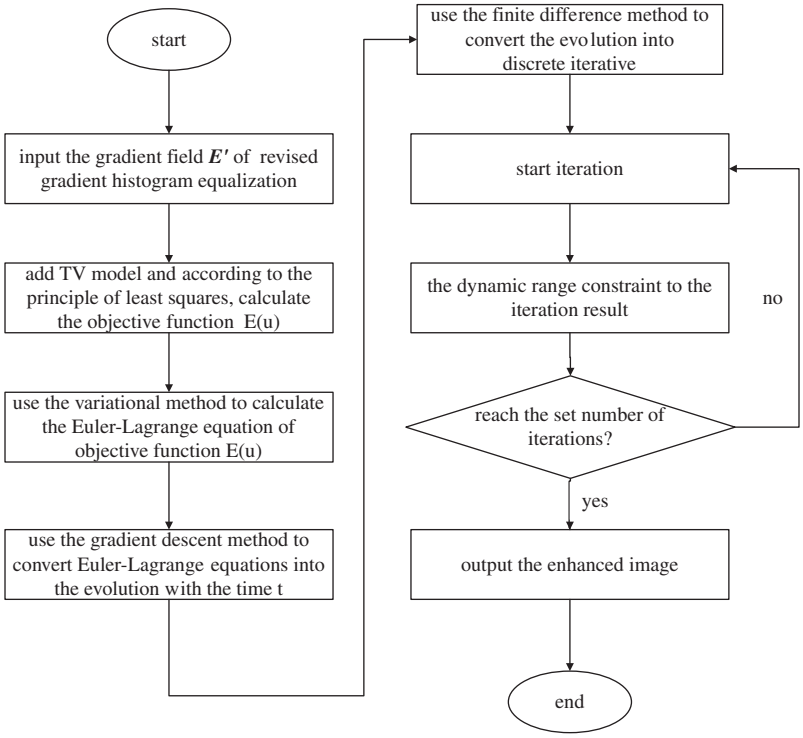

Fig. 4. The flowchart of image reconstruction.

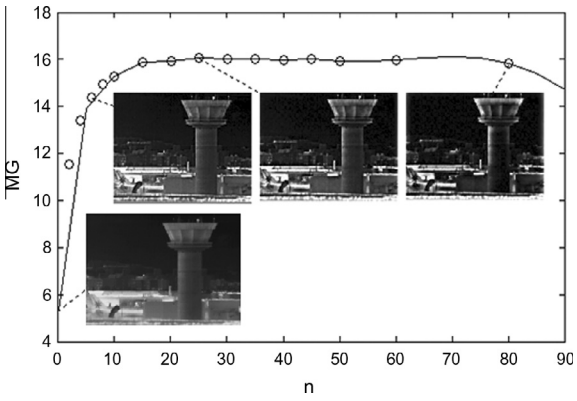

Fig. 5. The relation curve of MG-n.

If parameters χ and δ of (11) are with different values, there will be different effects between image edge detail enhancement and noise suppression. We take different parameter values for experiment and the result is shown in Fig. 7.

Fig. 7(a) is an infrared original image with dark background and big noise. From Fig. 7(b)–(d), with the increment of χ and the decrease of δ, noise suppression capability of the algorithm is improved while image edge detail enhancement capability is weakened. Comprehensively considering image edge detail enhancement and noise suppression of the algorithm, we take $\chi = 0.2$, $\delta = 0.8$.

In addition, to illustrate the effectiveness of revised gradient histogram equalization by adaptive dual thresholds, we compare the gradient histogram equalization algorithm with the revised gradient histogram equalization algorithm for infrared images. The results are shown in Fig. 8.

Fig. 8(a) is an original infrared image with low contrast and dim targets (stars) getting lost in the dark background. Gradient field equalization enhances infrared image targets, but enhanced image appears white spots due to the small gradient values excessively increased. This makes little stars buried in white spots as shown in Fig. 8(b). However, revised gradient histogram equalization by adaptive dual thresholds prevents image from excessive enhancement and dim targets are enhanced significantly as brighter stars as shown in Fig. 8(c). From the gradient histograms we can see that the gradient values of original image are mainly concentrated in 0–40. The revised gradient histogram equalization makes gradient values mainly concentrated in 0–120. While gradient field equalization makes the gradient values excessively increased to 0–255.

To further verify the effectiveness of the proposed algorithm, we compare it with HE, PHE [7] and infrared image enhancement based on wavelet diffusion (WD) [14]. Here are some experimental results.

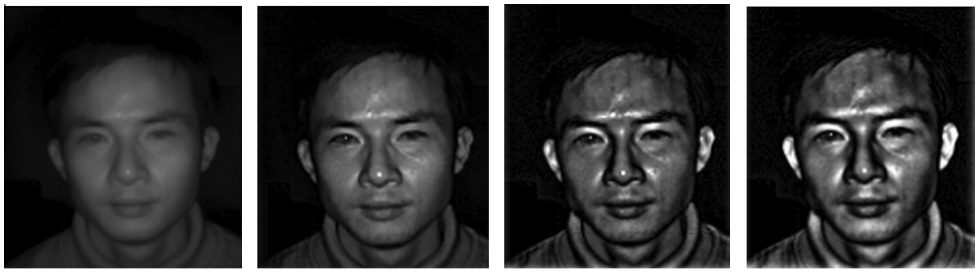

Fig. 6. Comparison of the infrared face image reconstructed by different M, (a) original infrared hand image, (b) $n = 6$, (c) $n = 25$ and (d) $n = 80$.

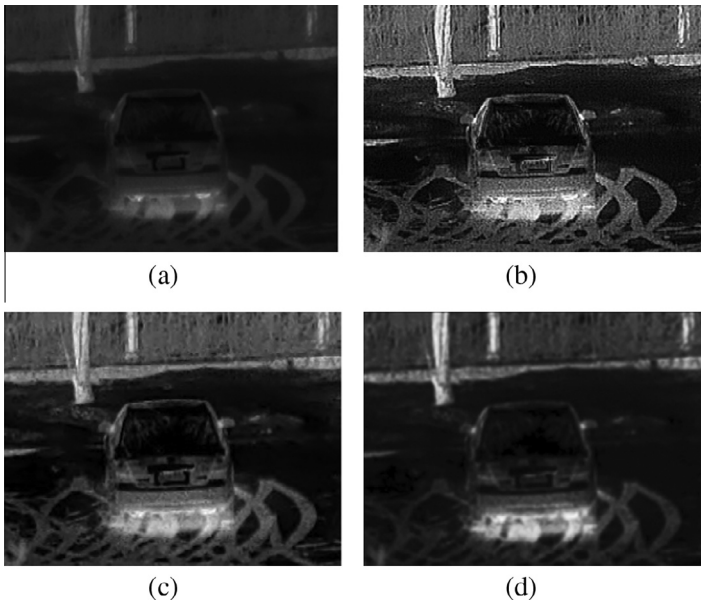

Fig. 7. Comparison of different values of χ and δ, (a) original infrared image, (b) $\chi = 0$, $\delta = 1$, (c) $\chi = 0.2$, $\delta = 0.8$ and (d) $\chi = 0.4$, $\delta = 0.6$.

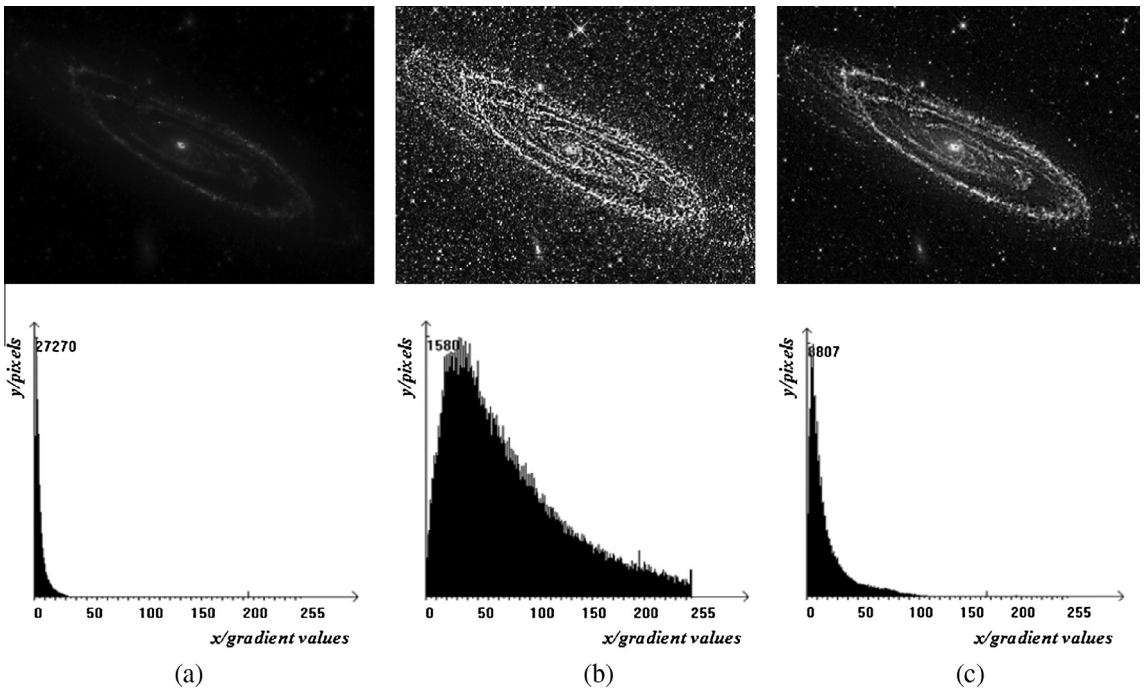

Fig. 8. Experiment about revised gradient histogram equalization, (a) original image and its gradient histogram, (b) gradient histogram equalization and its gradient histogram and (c) revised gradient histogram equalization and its gradient histogram.

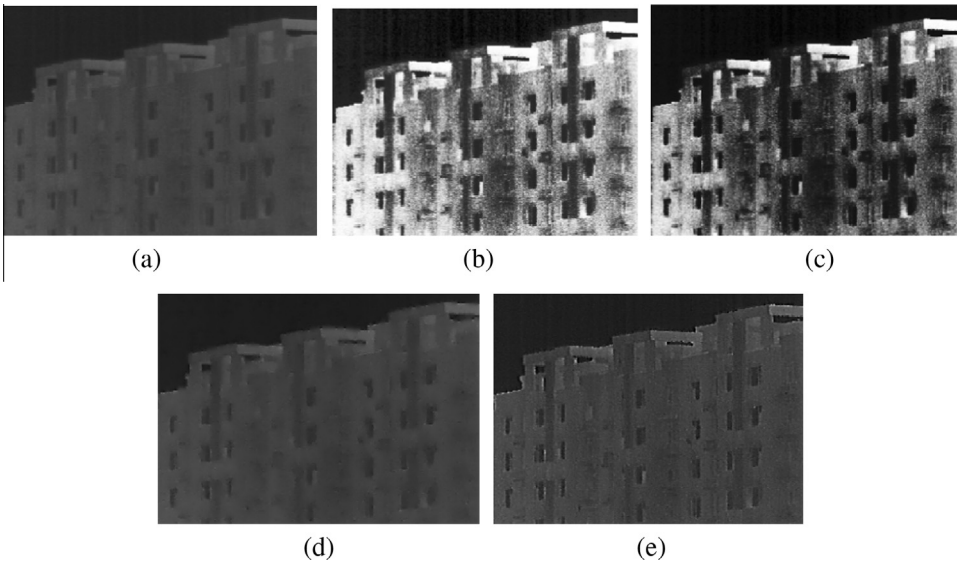

Fig. 9. Comparison of image enhancement results by different algorithms, (a) original image, (b) HE, (c) PHE, (d) WD and (e) the proposed algorithm.

Fig. 9(a) is an infrared original image with small signal-to-noise ratio and fuzzy texture edges. In Fig. 9(b), HE effectively extends the dynamic range of the image. However, it produces the over-enhancement. Using PHE, the image contrast is improved, and does not be over-enhanced as shown in Fig. 9(c). Fig. 9(d) is the result of WD. The texture edges are enhanced while suppressing noise. The result of the proposed algorithm is shown in Fig. 9(e). It can be seen that the image texture edges are clear.

Fig. 10(a) is another infrared original image, and the texture edges of the target ship are unclear. Using HE and PHE, the image contrast is improved, but the texture edges of the ship are not clear. The enhanced image by WD is shown in Fig. 10(d). The texture edges of the ship are clearer than Fig. 10(a). Fig. 10(e) is the result of the proposed algorithm, and the edge details of the ship are very clear.

Fig. 11(a) is a low dynamic range infrared image and the blood vessels and outline of the hand are not clear. HE and PHE expand the dynamic range, but the blood vessels and outline of the hand are not enhanced effectively. WD sharpens the blood vessels while suppressing noise. The image enhanced by the proposed algorithm is shown in Fig. 11(e). The blood vessels and outline of the hand are very clear.

In addition, the proposed algorithm can also be applied to enhance other types of images. Figs. 12 and 13 show the visible image and medical image enhanced by the proposed algorithm.

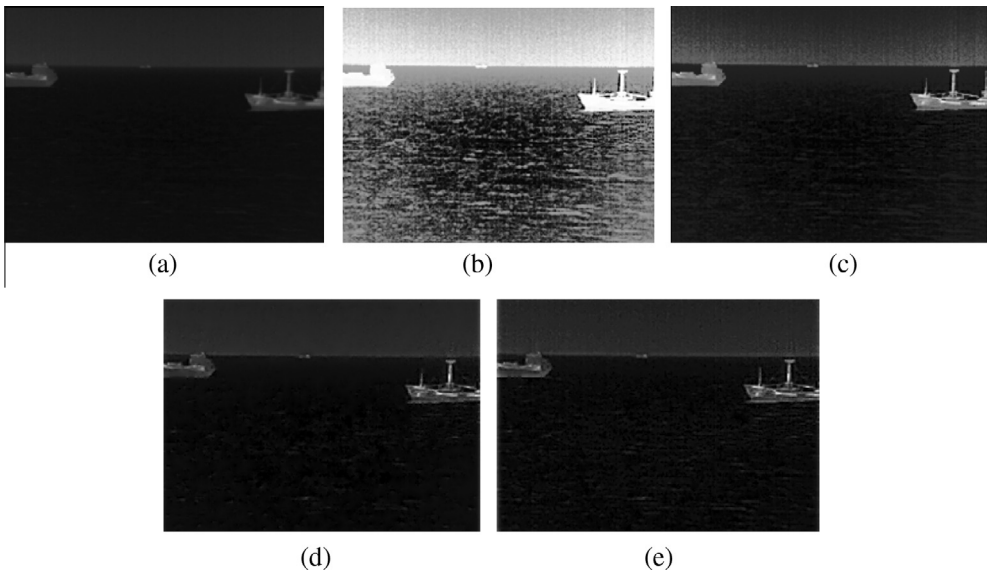

Fig. 10. Enhancement results comparison of ships by different algorithms, (a) original image, (b) HE, (c) PHE, (d) WD and (e) the proposed algorithm.

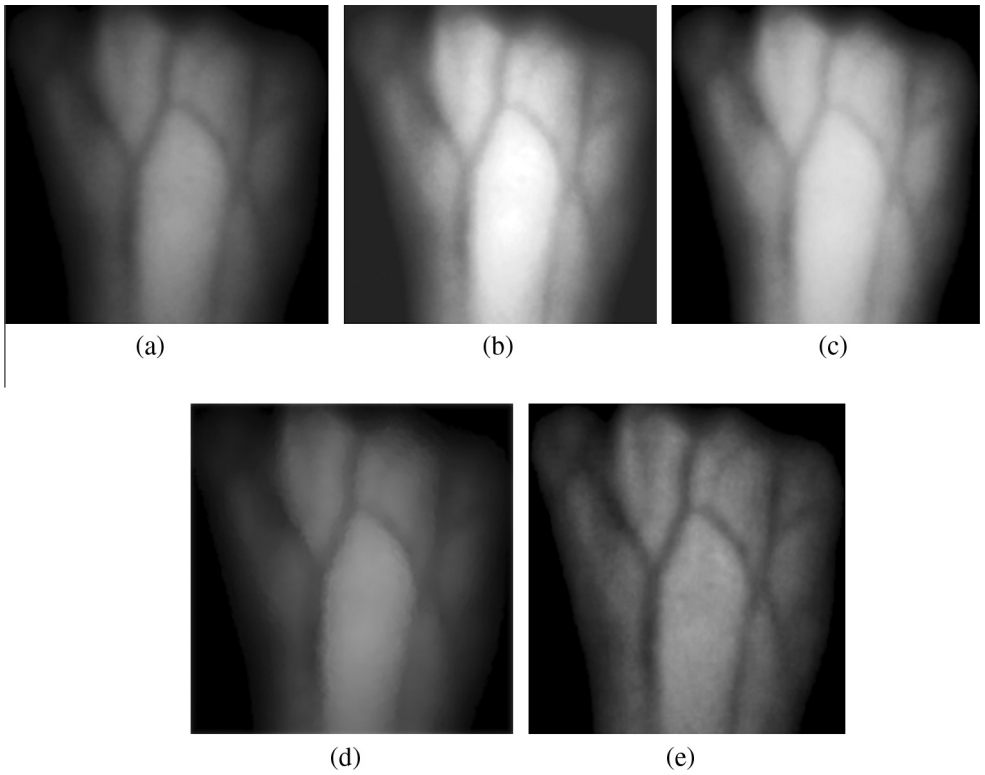

Fig. 11. Enhancement results comparison of hands by different algorithms, (a) original image, (b) HE, (c) PHE, (d) WD and (e) the proposed algorithm.

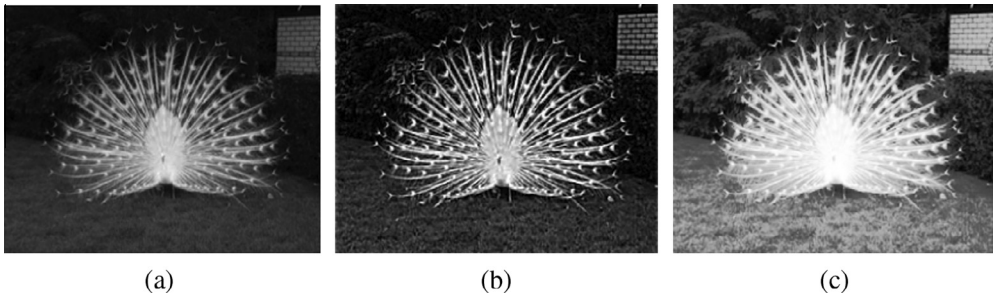

Fig. 12. The comparison of visible images enhancement, (a) original image, (b) the proposed algorithm and (c) HE.

(a) (b) (c)

Fig. 13. The comparison of medical CT images enhancement, (a) original image, (b) the proposed algorithm and (c) HE.

Fig. 12(a) is a visible peacock image, and the texture edges of the peacock are not clear. In Fig. 12(c), HE expands the dynamic range of the image, but it produces the over-enhancement. After the proposed algorithm, the texture edges of the peacock are well enhanced.

Fig. 13(a) is a medical CT image, and the details are not clear. In Fig. 13(c), HE increases the brightness of the image, but the details are not clear enough. After the proposed algorithm, image details and edges are clear.

The infrared images and other types of images have been applied in the experiment, and the edge details of the images are well enhanced. This shows that our algorithm can work well for various images.

4. Conclusions

We have demonstrated the infrared image enhancement by means of the total variation and gradient field equalization with adaptive dual-threshold. The gradient values of weak image details are low relative to other region, and we can increase the gradient values to enhance the weak detail information. Firstly, we introduce the principle of gradient field equalization. In order to prevent image from over-enhancement, considering the characteristics of infrared image, we set two thresholds to adjust the image gradient values. By adopting the TV model while reconstructing the enhanced image, the noise is suppressed. Experimental results show that the proposed algorithm effectively enhances infrared image edge details, which is beneficial to various applications of infrared images.

Conflicts of interest

There is no conflict of interest.

Acknowledgements

We thank the reviewers for helping us to improve this paper. This work is supported by National Natural Science Foundation of China (Grant No. 61137001).

References

[1] C.L. Lin, An approach to adaptive infrared image enhancement for longrange surveillance, Infrared Phys. Technol. 54 (2) (2011) 84–91.
[2] J.J. Talghader, A.S. Gawarikar, R.P. Shea, Spectral selectivity in infrared thermal detection, Light:Sci. Appl. 1 (24) (2012).
[3] V.M. Carlos, J.S.M. Francisco, E.G.S. Maria, Contrast enhancement of mid and far infrared images of subcutaneous veins, Infrared Phys. Technol. 51 (3) (2008) 221–228.
[4] K.S. Sim, C.P. Tso, Y.Y. Ta, Recursive sub-image histogram equalization applied to gray scale images, Patter Recognit. Lett. 28 (10) (2007) 1209–1221.
[5] H. Ibrahim, N.S.P. Kong, Brightness preserving dynamic histogram equalization for image contrast enhancement, IEEE Trans. Consum. Electron. 53 (4) (2007) 1752–1758.
[6] Q. Chen, L.F. Bai, B.M. Zhang, Histogram double equalization in infrared image, J. Infrared Millimeter Waves 22 (6) (2003) 428–430.
[7] R. Lai, Y.T. Yang, B.J. Wang, H.X. Zhou, A quantitative measure based infrared image enhancement algorithm using plateau histogram, Opt. Commun. 283 (2010) 4283–4288.
[8] K. Liang, Y. Ma, Y. Xie, B. Zhou, R. Wang, A new adaptive contrast enhancement algorithm for infrared images based on double plateaus histogram equalization, Infrared Phys. Technol. 55 (2012) 309–315.
[9] X.Z. Bai, F.G. Zhou, B.D. Xue, Infrared image enhancement through contrast enhancement by using multiscale new top-hat transform, Infrared Phys. Technol. 54 (2011) 61–69.
[10] J.F. Zhao, Y.T. Chen, H.J. Feng, et al., Infrared image enhancement through saliency feature analysis based on multi-scale decomposition, Infrared Phys. Technol. 62 (2014) 86–93.
[11] T.H. Yu, Q.M. Li, J.M. Dai, New enhancement of infrared image based on human visual system, Chin. Opt. Lett. 7 (2009) 206–209.
[12] P. Perona, J. Malik, Scale-space and edge detection using anisotropic diffusion, IEEE Trans. Pattern Anal. Mach. Intell. 12 (7) (1990) 629–639.
[13] S.J. Fu, Q.Q. Ruan, W.Q. Wang, F.Z. Gao, H.D. Cheng, A feature-dependent fuzzy bidirectional flow for adaptive image sharpening, Neurocomputing 70 (2007) 883–895.
[14] C. Ni, Q. Li, L.Z. Xia, A novel method of infrared image denoising and edge enhancement, Signal Process. 88 (2008) 1606–1614.
[15] L. Rudin, S. Osher, E. Fatemi, Nonlinear total variation based noise removal algorithms, Physica D 60 (1992) 259–268.
[16] T.F. Chan, S. Esedoglu, F. Park, A fourth order dual method for staircase reduction in texture extraction and image restoration problems, IEEE Int. Conf. Image Process. (2010) 4137–4140.
[17] X.Z. Bai, F.G. Zhou, B.D. Xue, Image fusion through local feature extraction by using multi-scale top-hat by reconstruction operators, Optik 124 (2013) 3198–3204.
[18] B. Klare, A.K. Jain, Heterogeneous face recognition: matching NIR to visible light images, IEEE Int. Conf. Pattern Recognit. (2010) 1513–1516.